On Flows Driven by Mechanical Stresses in a Two-Phase System

Yu. Gaponenko[1], I. Ryzhkov[2] and V. Shevtsova[3]

Abstract: Gas-liquid flows in annulus are analyzed for fluids in large range of viscosity ratios. The geometry corresponds to a liquid bridge co-axially placed into an outer cylinder with solid walls. The internal core consists of solid rods at the bottom and top, while the central part is a relatively short liquid zone filled with viscous liquid and kept in its position by surface tension. The gas enters into the annular duct and entrains initially quiescent liquid. The flow structures in the liquid and gas are obtained numerically for different shapes of solid rods. Solution for fully developed flow in annulus with moving core is found analytically. The regions, where the flow can be considered as locally fully developed, are identified by comparing numerical and analytical results. The role of mechanical stresses in the interface dynamics is examined and the optimal choice of supporting rods shape is discussed.

Keywords: two-phase flow, gas, liquid bridge, fully developed flow, interface.

1 Introduction

The dynamics of fluid systems involving interfaces remains a challenging problem of modern physics. The great majority of literature on adiabatic, isothermal, two-phase flow systems prior to the 1950th was devoted mainly to the demands of the oil fields.

At the same time, considerable interest was shown in the study of two phase flow with heat/mass transfer in relation to such applications as power generation and refrigeration. Nowadays, heat/mass transfer on the moving gas-liquid interface is an important subject directly related to many industrial applications from crystal

---

[1] ygaponen@ulb.ac.be;

[2] iryzhkov@ulb.ac.be;

[3] vshev@ulb.ac.be;

All authors: MRC, CP-165/62, Université Libre de Bruxelles, 50, av. F. D. Roosevelt,B-1050 Brussels, Belgium.

growth to cooling of electronic devices. In the present study, the attention is focused on flows in cylindrical geometry. Such systems have a large field of applications in the production of highest quality semi-conductors, fibers, micro-jets, etc.

The best quality crystals are grown by floating zone technique. Studies on the mechanisms governing the flow dynamics and heat transfer are particularly helpful in controlling the crystal growth process and thereby the quality of its products. The scientific model, which is used to mimic industrial floating zone technique, is called a liquid bridge. During last decades, a significant progress has been achieved in understanding nonlinear regimes of buoyant-thermocapillary convection in liquid bridges, see for example monographs by Kuhlmann (1999) and Lappa (2004). However, only recently it was recognized that the flow in surrounding gas phase and heat/mass transfer at the interface are important factors for the stability of flow inside liquid bridge. The experimental results were the first to indicate the extreme sensitivity of flow stability in liquid bridges to environmental conditions. Experiments performed in different configurations by Shevtsova *et al.* (1999, 2005), Mialdun & Shevtsova (2006) and Kamotani *et al.* (2007, 2007a) have demonstrated a similar tendency that ΔT_{cr} changes by a factor of two or three by varying the air temperature relative to the cold wall temperature.

The number of publications considering flow both in liquid bridge and surrounding gas is still very limited, see Irikira et al. (2005), Tiwari and Nishino (2007). As a rule, the flow is considered inside liquid, and the boundary conditions on the free interface capture the impact of surrounding gas through the Biot number, e.g. Melnikov et al. (2007). Note that experiments by Kamotani et al. (2003) have shown that the disturbances of gas flow near the interface produce significant impact on the stability of the liquid flow.

It is desirable to perform additional experimental studies on the threshold of instability with varying mechanical and/or thermal stresses at the interface (especially in microgravity environment where buoyant convection is almost absent). The Space experiment JEREMI (Japanese European Space Research Experiment on Marangoni Instabilities) is planned to be performed in 2012 in the Japanese Experiment module on ISS using the dedicated FPEF (Fluid Physics Experiment Facility). The experiment is aimed on investigating the influence of ambient gas on the behavior of free interfaces and fluid flow beneath. The behavior of the liquid flow under mechanical stresses produced by co- or counter flow of the ambient gas is one of the objectives to be studied.

The present study is one of the first and preliminary steps on the way of the experiment preparation. We provide insight into the role of mechanical stresses on the interface and analyze the optimal choice of supporting rods shape. In this paper, the emphasis is on isothermal, adiabatic two-phase gas-liquid flow in cylindrical geom-

etry without mass transfer in configuration where liquid zone has limited length.

The gravity effect is not included into consideration so the channel orientation is not important. In addition, this results remains valid for flow in the micro- and large nano-channels with cross-sectional diameters of the order 300-500 nm with one-two order of magnitude reduction in the hydrolic diameter, see Yarin et al. (2009).

2   Variety of the liquid bridge geometry

Sketches of different experimental set-ups generally used for studying flows in liquid bridges are shown Fig. 1. Here the internal parts are surrounded by co-axial cylindrical tube of radius R_{out}. Liquid bridge itself (shown by blue color) is a drop of liquid kept by surface tension between two differently heated rods. Usually, the system is heated from above. The temperature of the lower rod is either kept constant or decreased to maintain constant the mean temperature in the system. The thermocapillary flow arises in liquid for any temperature difference ΔT between the supporting rods. In ground conditions, this flow is modified by the buoyancy force.

Usually numerical studies consider only the flow inside liquid zone. However, experimental set-ups include rods of different lengths and configurations. Let us briefly describe the most popular once. *Type 1* has the simplest geometry, in which the cylindrical supporting rods do not have any grooves or protrusions. To prevent fluid from creeping over the edges of the rods, they have to be coated with an anti-wetting-barrier, which depends on the liquid and on the material of rods, Frank & Schwabe (1997).

To skip anti-wetting coating or to reinforce arrangement, the bottom rod is often processed into a sharp edge, e.g. see Shevtsova et al. (2005), Nishimura et al. (2005). This geometry corresponds either to *Type 2* or *Type 3*. The difference between them is not important for ground based experiments and choice belongs to the question of fabrication. However, *Type 2* is more functional for Space experiments, where liquid bridge should stay in operation by hours. A small creeping during experiment in *Type 3* will provoke accumulation of liquid inside groove, kept by surface tension. In long-duration experiments, it may provoke the breakage of a liquid bridge when liquid completely fills the groove. The process might be accelerated by on-board g-jitters. Both geometries allow manufacturing the upper rod from transparent sapphire for visual observations of flow patterns through the top.

In the experiments with large ΔT, while heating from above, the use of anti-wetting-barrier may be not sufficient for prevention of creeping. In this case, the grooves
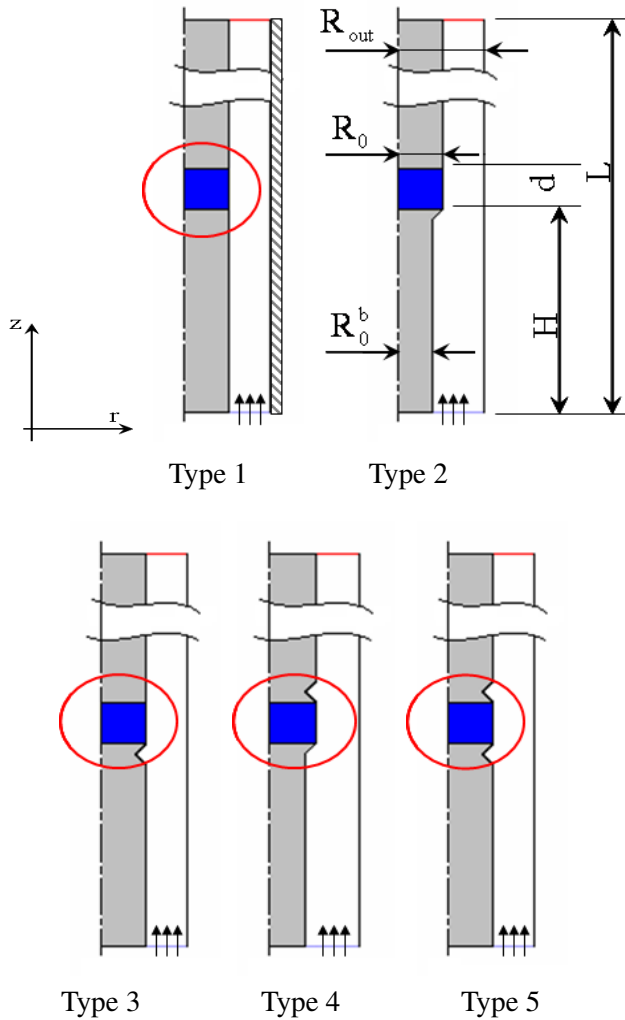
Figure 1: (online color) Sketches of different experimental set-ups used for studying of liquid bridges

are also made at the upper rod, see *Type 4* or *Type 5*. The latter one was used in experiments by Kamotani et al. (2003) and we plan to use it for a ground-based prototype. *Type 4* is a candidate to be used for future JEREMI experiment.

3 Formulation of the problem

To study the influence of mechanical stresses imposed on the interface, the various gases will be blown in the cylindrical channel with different velocities. Gas of constant flow rate Q_{in} flows through annular duct of outer diameter $r = R_{out}$ and inner diameter $r = R_0^b$, see notation in Fig. 1. Reaching the liquid zone after distance H from the tube inlet, it creates flow in quiescent liquid due to viscous stress. After passing the liquid zone of length d, gas continues to flow through annular duct of inner radius $r = R_0$ over the distance H up to the tube outlet. Subscript "b" stands for "bottom". The total length of the tube is $L = 2H + d$. The radius of liquid zone is R_0. The geometrical scales are given in Table 1. In addition, size of triangle protrusion/groove is $0.5mm$ in horizontal and vertical directions. We analyze the flow field in the gas and liquid for all five types of the set-ups presented in Section 2. The gas is assumed incompressible in consistency with the low pressure drop between the tube ends.

The dynamics of system in the geometry of Fig. 1 is described by the momentum and continuity equations for an incompressible Newtonian fluid in gas (^{g}) and liquid (^{l}) in cylindrical coordinates (r,z):

$$\mathbf{V^g} \cdot \nabla \mathbf{V^g} = -\frac{1}{\rho^g}\nabla P^g + \frac{\mu^g}{\rho^g}\nabla^2\mathbf{V^g} \tag{1}$$

$$\nabla \cdot \mathbf{V^g} = 0, \tag{2}$$

and

$$\mathbf{V^l} \cdot \nabla \mathbf{V^l} = -\frac{1}{\rho^l}\nabla P^l + \frac{\mu^l}{\rho^l}\nabla^2\mathbf{V^l} \tag{3}$$

$$\nabla \cdot \mathbf{V^l} = 0, \tag{4}$$

where the velocity $\mathbf{V} = [V, U]$ includes the radial V and axial U components; μ is the dynamic viscosity and ρ is the density.

Boundary conditions are:
on the liquid–gas interface $r = R_0$:

$$U^l = U^g, \qquad V^l = V^g = 0, \tag{5}$$

$$\mu^l \frac{\partial U^l}{\partial r} = \mu^g \frac{\partial U^g}{\partial r}, \tag{6}$$

on liquid bridge axis $r = 0$:

$$\partial_r U^l = 0, \quad V^l = 0, \tag{7}$$

on the wall of the external tube $r = R_{out}$:

$$U^g = 0, \quad V^g = 0, \tag{8}$$

no-slip conditions are also imposed on the supporting rods.

Inlet conditions between cylinders $z = 0$, $r = R_0^b < r < R_{out}$. During the experiments, external gas is blown into the cylindrical channel through a layer of porous media to avoid azimuthal motion of gas around the rod (kind of vortex tube). It will provide quasi-constant velocity at the inlet. Thus one can impose

$$U = U_0 = const, \quad V = 0 \tag{9}$$

or constant flow rate, calculated as $Q_{in} = U_0 \pi (R_{out}^2 - R_0^2)$.

Outlet conditions at $z = L$, $r = R_0 < r < R_{out}$. The flow velocity and pressure at the outlet are not known prior to solution of the flow problem. The zero flux conditions applied at outflow boundaries are approached physically in fully-developed flows, i.e. flows in which the flow velocity profile is unchanging in the flow direction.

$$\partial_z U^g = 0, \quad \partial_z V^g = 0 \tag{10}$$

Since these boundary conditions are artificially imposed, the outlet boundary is to be sufficiently remote from the liquid bridge to avoid numerical reflections. The question whether these conditions allow perturbations to penetrate back inside the tube will be discussed in Section 3.2.

Hereafter, the hydraulic diameter,

$$D_h = 2R_{out} - 2R_0, \tag{11}$$

will be used as characteristic length scale.

Table 1: Geometrical scales used in calculations, unless otherwise stated; $D_h = 4 \cdot 10^{-3} m$.

R_{out}	R_0	R_0^b	H	d	L
$10^{-3}m$	$10^{-3}m$	$10^{-3}m$	$10^{-3}m$	$10^{-3}m$	$10^{-3}m$
5	3	2.5 or 3	20	3	43

4 Fully developed flow in annulus; analytical solutions.

Let us consider the flow in duct between infinite coaxial cylinders when the inner wall is moving and the outer wall is motionless. The internal core has constant radius R_0. The fully developed flow of an incompressible Newtonian fluid in an annular channel in the cylindrical coordinates (r,z) shown in Fig. 1 is described by

$$-\frac{\partial P^g}{\partial z} + \mu^g \frac{1}{r} \frac{\partial}{\partial r}\left(r \frac{\partial U^g}{\partial r}\right) = 0 \tag{12}$$

The boundary conditions are :
$r = R_0, \ U = U_0^l, \qquad r = R_{out}, \ U = 0.$
The solution can be obtained in the form of an elegant algebraic expression

$$U^g = \frac{R^2}{4\mu^g} \frac{\partial P^g}{\partial z}\left[\left(\frac{r}{R}\right)^2 - 1 - \frac{\gamma^2 - 1}{\gamma^2 \ln \gamma} \ln \frac{r}{R}\right] - \frac{U_0^l}{\ln \gamma} \ln \frac{r}{R}, \tag{13}$$

where $R = R_{out}$ and $\gamma = R_{out}/R_0$ is the aspect ratio. In the absence of the velocity on the surface of internal cylinder, i.e. $U_0^l = 0$, the Eq.13 is reduced to the solution of the Poiseuille-type flow in annulus

$$U^g = \frac{R^2}{4\mu^g} \frac{\partial P^g}{\partial z}\left[\left(\frac{r}{R}\right)^2 - 1 - \frac{\gamma^2 - 1}{\gamma^2 \ln \gamma} \ln \frac{r}{R}\right], \tag{14}$$

which can be found in literature.

5 Numerical procedure

5.1 Solution method

One of the goals of the present study is to analyze the influence of rod shapes on the flow structure. It requires a complicated computational mesh. For convenience and with the aim of making our results readily reproducible by others, we have used the well-tested commercial solver FLUENT v.6.3 (laminar steady). The computational mesh generated by commercial code GAMBIT is depicted in Fig.2. The cells are mostly square and rectangular; near areas with shape change, they are triangles. In the liquid bridge area the mesh is square with the equal radial and axial length $\Delta z = \Delta r = 3.75 \cdot 10^{-5} m$ that corresponds 80 nodes in any direction. In the gas area the edge mesh has the stretch factor 1.05 and 50 nodes in any direction. Note that the smallest cells lie at the region of the liquid zone and around grooves/protrusions. In this region the smallest size mesh cell is $2 \cdot 10^{-5} m$.
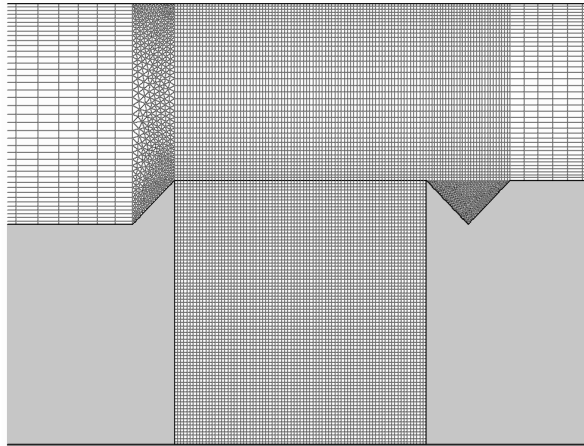
Figure 2: Grid of the central part of the considered domain for *Type 4* in horizontal layout. Denser mesh is provided in the areas adjacent to the channel shape change, near solid walls and interface.

An issue requiring consideration is the treatment of the interface. Using standard FLUENT option VOF or two-phase flow appears to be extremely slow. The problem was treated iteratively performing calculations at one time only in a single phase. The solutions were coupled through continuity of velocity and shear stress boundary conditions. At first step the flow in gas phase is calculated considering internal cylinder as rigid. At the output a viscous stress $\tau^g = \mu^g \partial_r U^g$ is calculated at the area of liquid bridge location. At the 2nd step the flow inside liquid bridge is calculated using the known viscous stress as boundary condition $\tau^l(r = R_0) = \tau^g = \mu^l \partial_r U^l$. The output of this step is the velocity distribution on the free surface, $U = U_l(r = R_0)$. On 3rd step the flow in gas phase is again calculated with prescribed value of velocity on the interface. This procedure is considered as one iteration. The solutions converge rather rapidly. The maximal difference between two successive iterations for the velocity on the free surface for the worse case ($U_0 = 0.25$ m/s, Type 4) is

$$max|(U^l_{1it} - U^l_{2it})/U_0| = 2.1 \cdot 10^{-5},$$
$$max|(U^l_{2it} - U^l_{3it})/U_0| \leq 1.0 \cdot 10^{-8}.$$

As a rule after third iteration the calculations were stopped. The similar approach, i.e. using coupling of solutions for flows in two different fluids was successfully used for treating near-interface turbulence by Lombardi et al (1996).
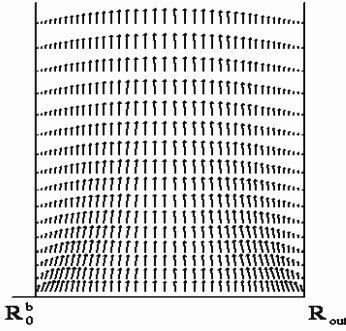
Figure 3: Development of Poiseuille profile when $U_0 = 0.05 m/s$. Velocity field near the tube inlet.

5.2 Validation of the numerical results

The use of commercial code does not give guarantee of obtaining the physically correct results. Validation of results is done by comparison with Poiseuille profile in coaxial cylinders, when the entire internal part is solid. Once gas enters into an annular channel with velocity $U = U_0^g$, the fluid in contact with the walls basically stops while the fluid away from the wall surface continues to move. Close to the inlet region, significant viscous effects will be concentrated in the thin boundary layers near the solid walls. Moving further into the pipe, these boundary layers will increase in thickness until they reach a point where they merge, so that the whole fluid is significantly affected by viscosity. Poiseuille profile is developing and fully developed flow has its onset, see Fig. 3. For the case of fully developed flow (similar to that in infinite cylinders), the solution was obtained analytically, see Section 4.

To check validity of outlet boundary conditions (Eq. 10) the flow was examined at that region for all five types of geometries in Fig. 1. For the largest considered inlet velocity, $U_0 = 0.25$ m/s, the numerical solutions were compared with fully developed (FD) profile. The analysis showed that approaching the outlet above liquid bridge, $z \approx 0.8 - 0.9 L$, the FD profile is re-established. However closer to the outlet, $z \approx 0.95 L$, a small difference re-appears. There is no physical reason for this difference except boundary conditions. Therefore, we have performed simulations with extended upper part, $z = L + H/2$, to minimize artificial boundary effects in the results obtained. The results below are analyzed for initially prescribed length, $0 < z < L$, and extended zone is not under discussion.

For validation of results, the calculations have been performed in extended geometry when the internal circular core is solid and inlet velocity is $U_0^g = 0.05 m/s$. The results were compared with analytical solution, Eq. 14, where pressure drop
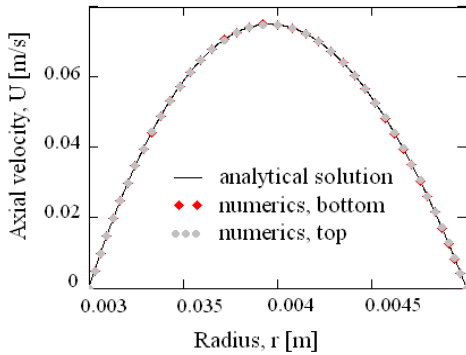
Figure 4: (online color) Comparison of velocity profiles obtained numerically and analytically for fully developed flow.

was taken from the results of calculations, $\partial P^g/\partial z = -2.668$ Pa/m and $\gamma = 5/3$. Figure 4 shows the axial velocity U: a) near the inlet $z = 0.12L$ by red rhombus; b) near the outlet $z = 0.98L$ by grey circles and c) the analytical solution, Eq. 14, by solid line. They are practically indistinguishable at the presented scale. The maximal difference near the inlet is located near the rigid walls ($r = 3.17$mm and $r = 4.35$mm) and its value is

$$max \frac{|U_{Eq.13} - U^g_{z=0.12L}|}{U^g_0} \approx 1.7 \cdot 10^{-4}.$$

Close to the tube outlet the maximal difference occurs at the middle of the duct and its value is

$$max \frac{|U_{Eq.13} - U^g_{z=0.98L}|}{U^g_0} \approx 2.0 \cdot 10^{-4}.$$

Thus, in the case of rigid core only 5mm from the inlet $(0.12L/R_{out} \approx 1)$ the flow has well developed Poiseuille type profile.

6 Discussion

6.1 *Flow structure in gas*

For a two-phase system of a liquid entrained by gas, different internal flow structures can occur depending on the size or shape of the flow channel, the magnitudes of the gas flow parameters, and on the physical properties of the two phases. In addition to the geometrical scales given in Table 1 the physical properties of working fluids are summarized in Table 2.
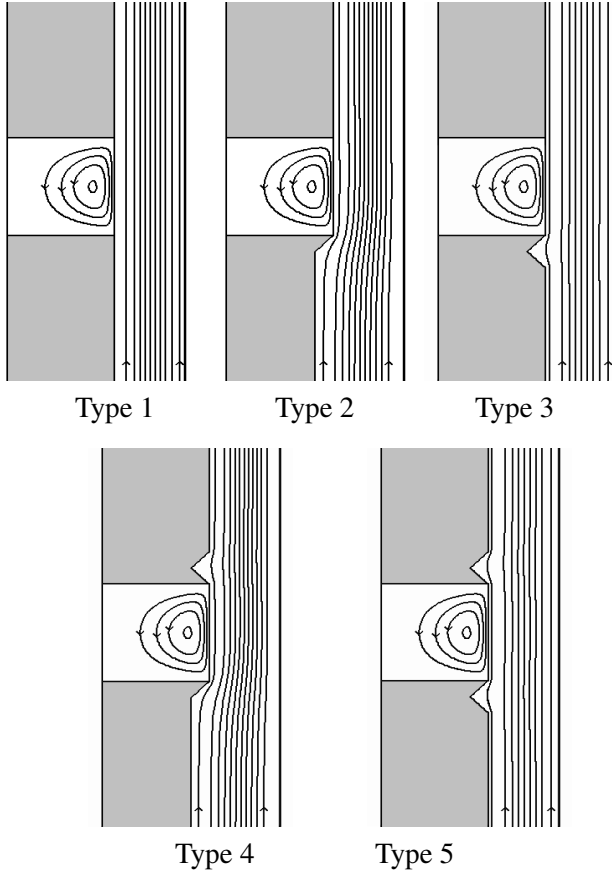
Figure 5: Flow patterns at different geometries in 5 cSt silicone oil/air system when $Q_{in} = 12.57 \cdot 10^{-6}\, m^3/s$

Table 2: Physical properties of the fluids.

	$\mu,\, Pa \cdot s$	$\rho,\, kg/m^3$	μ/μ_{air}
air	$17.9 \cdot 10^{-6}$	1.25	1
neon	$31.3 \cdot 10^{-6}$	0.90	1.75
ethanol	$1.084 \cdot 10^{-3}$	785	60.6
5cSt silicone oil	$4.56 \cdot 10^{-3}$	912	255
acetone	$3.31 \cdot 10^{-4}$	791	18.5

The analysis of gas flow was done for 5 cSt silicone oil and air, while the study of the flow in a liquid phase was performed for the large variety of systems listed in Table 2.

The flow patterns for different geometries are shown in Fig. 5 for the same flow

rate at inlet, $Q_{in} = 12.57 \cdot 10^{-6} m^3/s$. As a general trend gas flow is laminar and unidirectional without large recirculation zones. Small recirculation cells exist inside all angle-shaped grooves (*Types 3, 4, 5*), but they are not visible on the chosen scale. The most perturbed flow structures are observed in the cases with conical shape of protrusions at lower part (*Types 2, 4*), where $R_0^b < R_0$. Note, that the initial velocity U_0 for this shape is smaller as duct size $D_h/2$ is larger, i.e. $U_0 = 0.213$ m/s for *Types 2, 4* while $U_0 = 0.25$ m/s for *Types 1, 3, 5*. More detailed analysis of the gas flow structure indicates that the disturbances penetrate downstream below the liquid zone.

Figure 6 shows an axial velocity in the center of the duct at $r = D_h/4$ when z varies between two segments with fully developed flow. Tracking the curve for conical shape of protrusion (upper plot) shows that velocity feels upstream disturbances below liquid zone at $z \approx 0.85\,H$ $(0.017\,m)$, which provoke at first tiny diminution of the velocity and then noticeable increase. Due to inertial effects the velocity begins to rise up before entering to the narrower part, which starts at $z = 0.975\,H$ $(0.0195\,m)$. Further, when entraining liquid, the gas velocity decelerates (see dashed part of the curve). Passing the liquid zone the channel becomes wider due to the groove at upper part and it leads to local decrease of velocity. Behind the groove the fully developed flow is again established.

The evolution is different in the case of two angle-shaped grooves, see bottom graph at Fig. 6. In *Type 5* the flow feels upstream perturbations closer to liquid zone than in *Type 4*. There exists two drop-jumps on the velocity profile at the
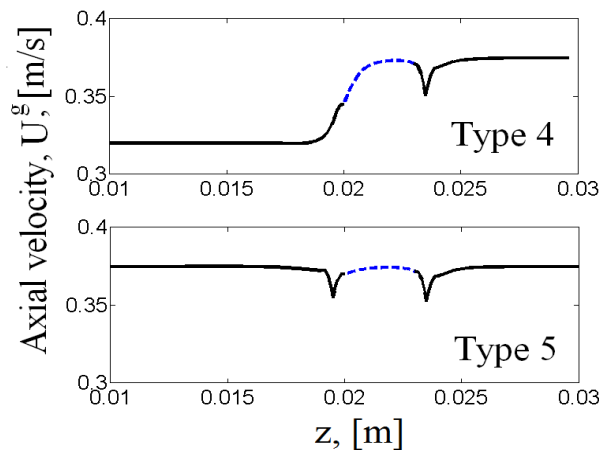

Figure 6: Axial velocity in z-direction in the middle of the duct, $r = D_h/4$ for *Types 4, 5*. Dashed curve depicts z-area parallel to the liquid zone.
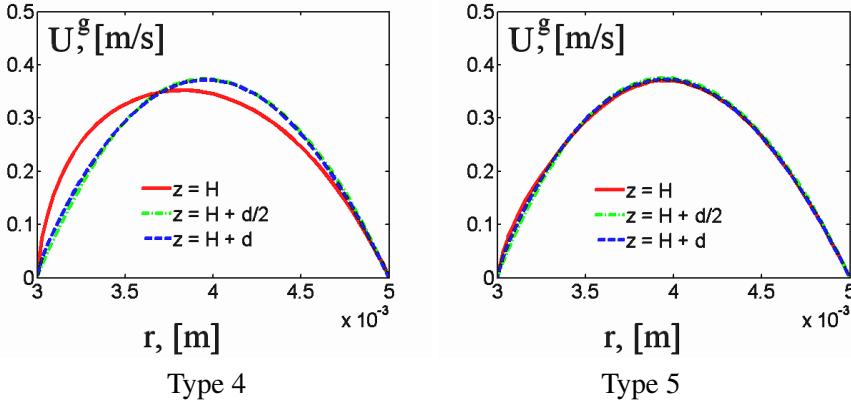
Figure 7: Axial velocity $U^g(r)$ at the beginning, $z = H$, middle, $z = H + d/2$, and at the end, $z = H + d$, of liquid zone; $Q_{in} = 12.57 \cdot 10^{-6}\, m^3/s$.

grooves location. The velocity drops down due to inertial effects, as the duct size locally increases in radial direction. Note, that flow disturbances propagate below and above grooves in non-symmetrical way.

The above analysis considers velocity evolution in gas phase along the central line. The flow in radial direction locally loose symmetry near the liquid bridge. In Fig 7 the axial velocity distribution in radial direction $U^g(r)$ is shown at different heights along liquid zone: at the beginning, middle and at the end. The axial velocity is not equal zero at the interface, $r = R_0 = 3mm$, but it is two order of magnitude smaller than $\max(U^g)$. Thus it is not distinguishable in given scale. For *Type 4* the velocity profile at the beginning of liquid zone, $z = H$, is strongly asymmetric: maximum velocity is smaller and shifted to the internal core. However at the mid-height of liquid bridge this asymmetry already disappears.

It is worth observing that for *Type 5*, rod with two grooves, the velocity profiles do not change much over length of the liquid zone. All velocity maxima are located at the same radial position r_{max}, which is very close to that in the case of fully developed flow (from Eq. 13):

$$r_{max} = \sqrt{\frac{U_0^l}{\ln \gamma} \frac{2\mu}{\partial P/\partial z} + \left(1 - \frac{1}{\gamma^2}\right) \frac{R_0^2}{2 \ln \gamma}}. \tag{15}$$

According this formula the maximum is only slightly shifted to the core from center of duct ($r_{max} = 3.95$), with increase of the liquid velocity U_0^l the shift becomes stronger.

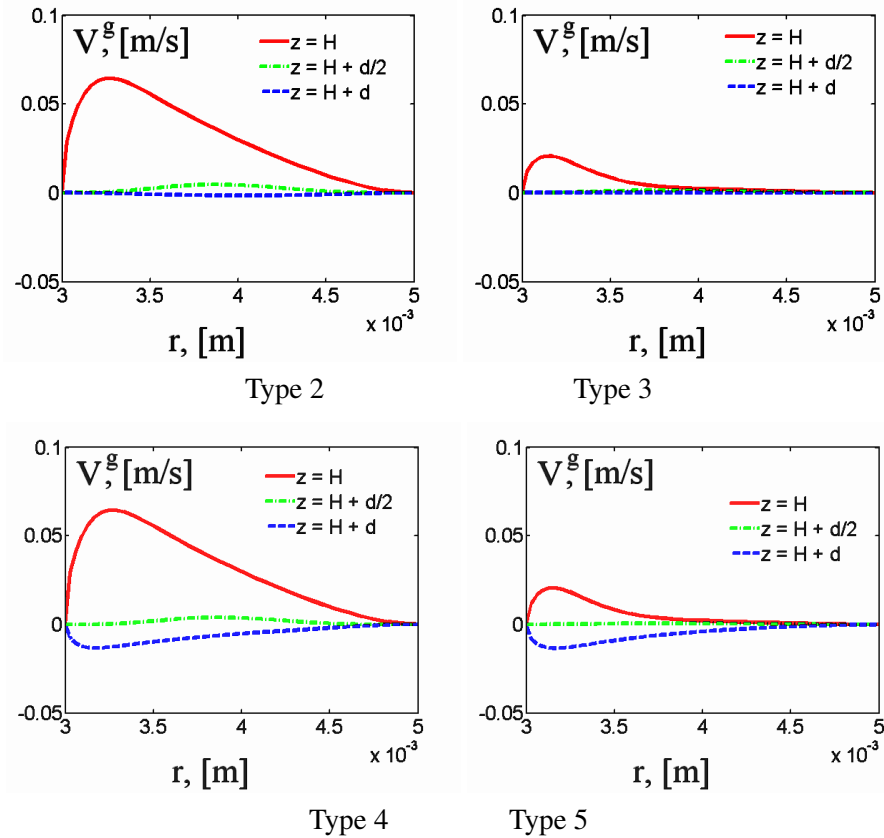Interestingly, that for all the shapes the maximal axial velocity at the end of liquid

Figure 8: Radial velocity in gas $V^g(r)$ at the beginning, $z = H$, middle, $z = H + d/2$, and at the end, $z = H + d$, of liquid zone; $Q_{in} = 12.57 \cdot 10^{-6} \, m^3/s$.

zone is roughly similar. One may compare blue curves for the most distinctive two cases (*Type 4, 5*) in Fig. 7, other ones are not shown. Over this study the maximal values were calculated for different inlet velocities, $0.01 \leq U_0^g \leq 0.25$ m/s and the data are summarized in Table 3 (*Type 5*). The values of Reynolds number, $Re = \rho U_0 D_h / \mu$, vary from $Re \sim O(1)$ to $Re \sim O(100)$, and for latter once the inertial effect can be important. Last column shows that the maximal axial velocity at the end of liquid bridge normalized by inlet velocity is almost constant for flow rates under consideration : $max[U_{z=H+d}^g(r)]/U_0^g \approx 1.49$.

Hence, the flow structure is developing in linear regime.

Table 3: Maximal U^g for different flow rates at $z = H + d$; water-silicone oil system

$Q_{in} \times 10^{-6}$ m^3/s	U_0 $[m/s]$	Re	$\max(U^g)$ $[m/s]$	$\max(U^g)/U_0$
0.503	0.01	2.8	0.0147	1.47
2.51	0.05	14.0	0.0746	1.492
12.57	0.25	70.0	0.372	1.488

6.2 Flow regimes

Typically for two phase gas-liquid system, the main task is to determine the physical properties of fluids and flow parameters at which the transition from one flow pattern to another will take place, so-called flow map regimes. For considered set of parameters, we may quantify zones where the flow regime can be considered as "locally fully developed".

The level of flow perturbations associated with the shape of the rods can be analyzed on the basis of radial velocity magnitude. In the case of fully developed flow, see Eq. 13, the radial velocity is equal to zero. Hence, the smaller is the radial velocity in the gas, the smaller is the level of perturbations. Figure 8 shows radial distribution of gas velocity $V^g(r)$ at different locations along the liquid zone. Velocity profiles for *Type 1* are not shown as they are rather small and cannot be seen in a given scale. All graphs reveal a general trend that maximum of $V^g(r)$ is shifted towards the liquid interface $r = R_0$ and the strength of perturbations is minimal at mid-height (green lines). Figure 8 clearly indicates that the upstream disturbances (below liquid zone) shown by red curves are larger in the presence of conic protrusion on the bottom part, i.e. *Type 2, 4*. Comparison of blue curves ($z = H + d$) for *Type 4, 5* reveals that level of downstream perturbations is almost similar in these geometries and the flow in that region is not visibly affected by prehistory, i.e. by the protrusion/groove shape at the lower part.

On the basis of the above study, the flow regime map, which identifies transitions between fully developed flow and simple forced flow, can be suggested. Figure 9 shows the flow regime map, where non-shaded areas corresponds to fully developed flow for the inlet velocity $U_0^g = 0.21 - 0.25$ m/s. There is an evident hydrodynamic entrance length L_e, where the flow is developing. Based on the analytical and experimental investigations available up to date, the best estimate of the entrance length L_e for laminar flow in circular pipes is:

$$L_e/D = 0.6 + 0.056\,Re,$$

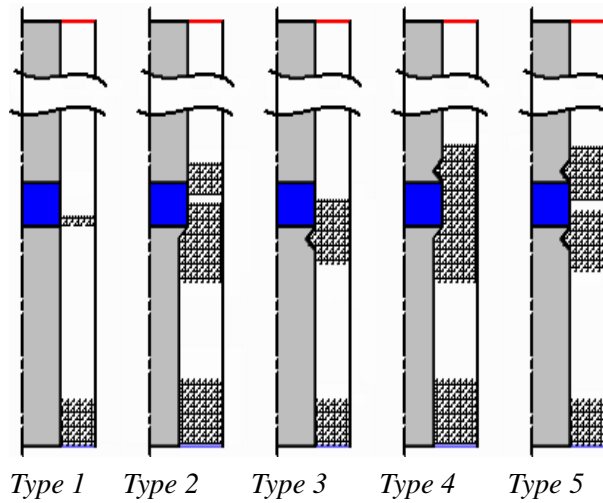where D is a pipe diameter, see Schetz and Fuhs (1999).

Type 1   Type 2   Type 3   Type 4   Type 5

Figure 9: Flow regime maps $Q_{in} = 12.57 \cdot 10^{-6} \, m^3/s$.

For our particular geometry, the parabolic profile forms inside the duct size $D_h/2$, which should be taken as characteristic length. This estimate does not work well for small velocities, but it gives correct trend that $L_e < 10$ mm for the largest Reynolds number in Table 1.

The important point of this estimate and numerical calculations, which give $5 \, mm < L_e < 10 \, mm$, is that for typical experimental set-ups the entrance length is small enough and does not influence the flow near liquid zone. Protrusion/groove shape plays pivotal role in the flow structure in the vicinity of the liquid bridge. As a rule, thermocapillary flows in liquid are studied on the length of liquid zone using sophisticated in-house made codes. Correct inlet and outlet boundary conditions are an important issue for comparison with the experiment.

Figure 9 shows that in the case of flat rods *Type 1* the flow is unperturbed except small area in the beginning of liquid zone. For this shape with a good tolerance the fully developed profile could be used for boundary conditions. For other shapes the flow is perturbed below and above liquid zone. The largest perturbation of gas flow occurs in system of *Type 4*.

6.3   *Pressure drop*

The pressure difference in examined system is caused by two main effects: due to changes of the channel cross-section and due to dynamic effects. For considered Reynolds numbers the viscous pressure drop is dominant although inertial (Bernoulli) pressure drop is not negligible when $Re \rightarrow 100$. The flow is locally fully developed (FD) inside two segments, below and above liquid bridge, but not

at the entrance region and transition region between segments where significant velocity changes occur. Figure 10 shows the calculated pressure drop between non-perturbed regions on different sides of liquid zone. In a given scale, the pressure drop is roughly a linear function of the inlet velocity. Our analysis includes large inlet velocities, $V = 0.25$ m/s, and as a consequence, it is difficult to see the small variations between the curves for different geometries.

Nevertheless for each particular velocity the pressure drop is not constant along the liquid zone. Here two effects can be underlined: change of channel size and shape effect. In fully developed flow, the pressure is a linear decreasing function and the value of the pressure gradient (pressure drop per unit length) is constant ($\Delta p / \Delta z = const < 0$). For the region of interest, pressure along the axial cooordinate looks like piecewise linear curve where different sections have different slopes. To follow the transitions near the liquid zone, we analyze not the pressure drop between the ends, but the local pressure gradient. Each change of the slope on the pressure curve will result in a drop-jump of the pressure gradient. Figure 11 shows this "local" pressure drop for three different shapes along the annulus. Hereafter the evolution of the pressure gradient will be discussed in terms of its absolute value. To make picture clear, only three geometries are shown in Fig. 11. Two vertical lines depict the location of the liquid zone in the core. For all geometries, near the entrance $|dp/dz|$ decreases approaching constant value, which corresponds to FD flow.
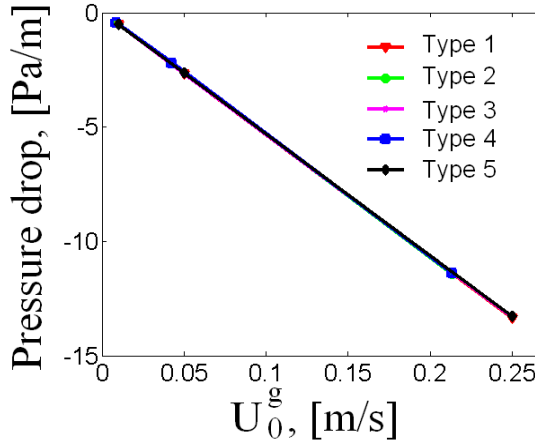

Figure 10: Pressure difference between top and bottom $\Delta P / \Delta z$ as a function of the entrance velocity. Δz is a distance between two sections with "locally" fully developed flow.
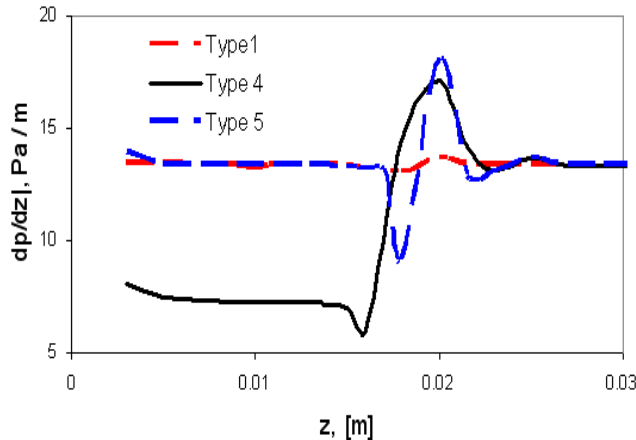
Figure 11: Pressure gradient over the annulus length for different geometries of rods

Tracking the pressure gradient in geometry *Type 4* shown by solid (black) line reveals that it lies higher than others as hydraulic diameter D_h near the bottom is larger. When approaching the protrusion, an asymmetrical flow pattern forms as weak perturbations penetrate downstream. Though the velocity change is very weak at this region, the pressure gradient reveals a small drop on the curve. Entering the narrower part, the velocity rises up, see Fig 6. Inertial effect becomes important, the pressure slope is changing, and pressure gradient starts to increase. Being in agreement with velocity profile (Fig 6), $|dp/dz|$ increases, reaches its maximum slightly inside the liquid zone and then goes down. At the end of the liquid zone, the flow is influenced by the upper groove. It provokes local decrease of the velocity and the pressure gradient reacts by small twist on the curve. Further the flow gradually undergoes transition to the fully developed one.

Tracking $|dp/dz|$ in geometry *Type 5* shown by dashed (blue) line demonstrates different behavior. Below liquid zone, a drop of $|dp/dz|$ is much larger than in *Type 4*, and it is located closer to the liquid. This drop-jump is provoked by local diminishing of the axial velocity because of the low groove. The following drop on the curve is caused by viscous stresses at the interface. The final twist is induced by the second groove above liquid zone. It has much smaller amplitude than previous once.

The dynamics of pressure gradient in flat geometry (*Type 1*) shown by dashed-dotted (red) curve is almost similar to the FD flow except small area below the liquid zone.

Certainly, for the same flow rate (inlet velocity) the pressure drop depends on cross-
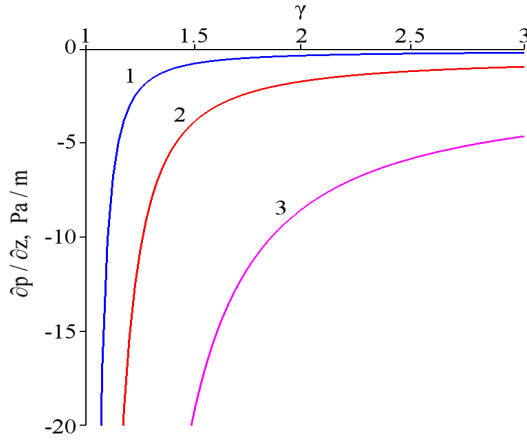
Figure 12: Pressure drop as a function of the aspect ratio, $\gamma = R_{out}/R_0$. Curves 1,2,3 corresponds to different flow rates $Q_{in} = (0.503, 2.51, 12.57) \cdot 10^{-6} m^3/s$.

section of the channel. Figure 12 shows pressure drop as a function of aspect ratio $\gamma = R_{out}/R_0$ for the flow rates. The curves 1-3 correspond to the different flow rates listed in Table 3. Here R_{out} is fixed while R_0 changes. The curves in are obtained on the basis of Eq. 13 when interface velocity is $U_0^l = 10^{-2} U_{max}^g$. For aspect ration $\gamma = 5/3$ the results are in excellent agreement with the data in Fig. 10. The conclusion out of this figure is that for the larger flow rate one needs wider duct to keep the same pressure drop in the system.

6.4 Flow structure in liquid

One of the goal of the study is to examine the role of mechanical stresses in the interface dynamics. The motion inside quiescent liquid is created by gas flow through viscous stresses. The rate of exchange of momentum between gas and liquid phases depends on the size and shape of the flow channel, the length of interfacial area, the ratio of viscosities, and the gas flow parameters.

Gas entrains the liquid on the interface and one vortex flow structure develops in the bulk, see Fig. 5. In the case of the large viscosity ratio, i.e. $\mu_{oil}/\mu_{air} = 255$ for air - 5cSt silicone oil, the resulting motion in liquid is rather weak even for relatively high flow rates ($Re \sim 100$). Figure 13 shows axial and radial velocity inside liquid as a function of r for all geometries. Comparison between axial velocities in liquid (Fig. 13) and gas (Fig. 7) reveals the difference of two orders of magnitude.

Figure 13a shows that for examined set of parameters, the axial velocity profile does not strongly depends on the geometry of the rods. The maximum of axial velocity reaches at the interface. The point where velocity changes the sign, $r \approx$
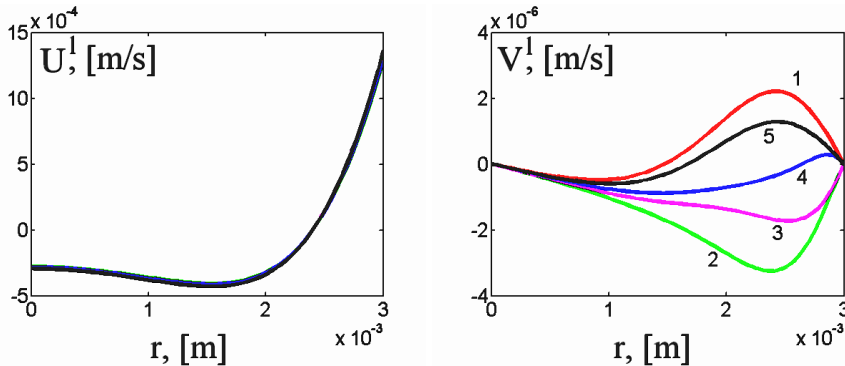
Figure 13: Velocity inside 5cSt silicone oil at mid-height $z = H + d/2$ for different shapes of rod: (a) axial velocity; (b) radial velocity ; $Q_{in} = 12.57 \cdot 10^{-6}\, m^3/s$.

$0.78 - 0.8 R_0$, characterizes the vortex center. However, the location and maximum value of the radial velocity is different for various geometries, see Fig. 13b. The location of $max|V(r)|$ indicates more precisely the position of the vortex center: is it shifted to the bottom or to the top.

The viscosity ratio plays a crucial role on the flow intensity in the liquid. Figure 14 shows velocity profiles on the interface for the same flow rate at different two-phase systems: air-silicone oil; neon-silicone oil; air-ethanol; air-acetone. It clearly demonstrates that velocity increases when the viscosity ratio diminishes for the same gas flow rate. The viscosity ratio strongly influences not only the value of the velocity but the flow structure as well. For large viscosity ratios the center of vortex is located in the middle of liquid zone, while for smaller once it is shifted in the direction of gas flow.

Figure 15 shows the maximum value of the interface velocity as a function of the viscosity ratio. On one hand the flow enhancement, when the ratio μ_l/μ_{gas} diminishes, is expected because as the liquid is driven by viscous stresses. On the other hand the rate of decrease is unexpectably strong, especially taken into account the limited length of interfacial contact. Thus to conclude, mechanical stresses imposed by gas blowing can create significant motion in a liquid depending on viscosity ratio.

7   Conclusions

Two-phase flows in annulus are analyzed for fluids in a large interval of viscosity ratios. The problem is solved numerically in complex geometry, which corresponds
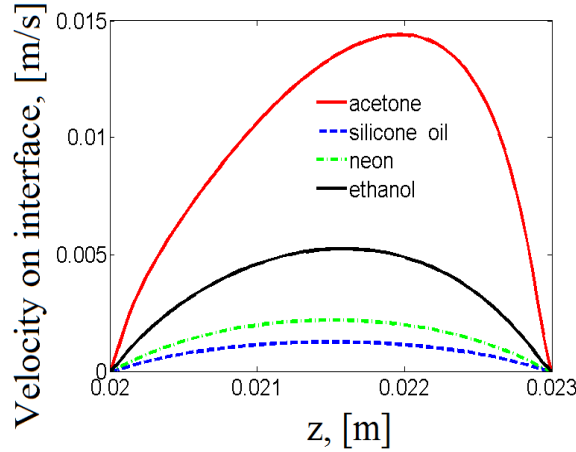
Figure 14: Velocity profiles on liquid interface driven by gas flow for different gas/liquid systems; Type 5, $U_0^g = 0.25 m/s$.

to a liquid bridge axially placed into an outer cylinder with solid walls. The internal core consists of solid rods with grooves and protrusions at the bottom and top, while the central part occupied by liquid is relatively short. The air enters into the annular duct and entrains initially quiescent liquid. The flow rate was varied in such a way that analysis includes both viscous and inertial effects, $2.8 < Re < 240$. The flow structure in the liquid and gas was examined for five most typical experimental geometries of the solid core. The configuration, in which the cross-sections of annular channel at the entrance and along the liquid zone are different, produces the strongest perturbation in gas flow. In the case of flat supporting rods, the gas flow can be considered as fully developed. Solution for fully developed flow in annulus with moving core is found analytically. The obtained flow regime maps show the areas, where the gas flow can be considered as fully developed.

It was found that the pressure difference between top and bottom areas, where the gas flow is "locally" fully developed, is a linear function of flow rate (inlet velocity). However, the detailed analysis indicates that near the liquid zone the pressure gradient is sensitive to the shape of the annulus (the supporting rods change the velocity of gas).

The analysis has shown that mechanical stresses imposed by gas blowing induces the motion of liquid. The enhancement of this flow depends on the viscosity ratio, gas flow rate, interface length, etc. One of the pivotal characteristics is the viscosity ratio which can be changed for the developed experimental set-up. The flow structure in liquid phase has been studied when viscosity ratio μ_l/μ_{gas} is changing
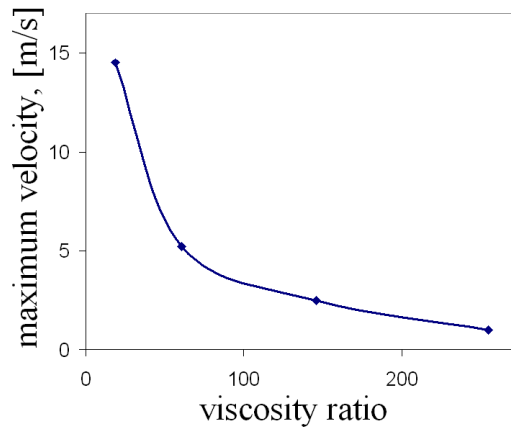
Figure 15: Maximal velocity of liquid versus viscosity ratio, μ_l/μ_{gas}; Geometry Type 5

from 18 to 255. The flow intensity in liquid strongly increases when viscosity ratio decreases.

We have also discussed how the present problem can be developed further by taking into account thermocapillary effects. In this case, configuration with flat rods (*Type 1*) can be calculated only on the length of liquid zone with Poiseuille profile as the boundary conditions for gas at the inlet and outlet. For other geometries, more sophisticated models are desirable.

Note, though the problem was considered in a specified geometry, the results can be interesting for a wide research community. The trends obtained in the analysis of viscosity ratio and pressure drop effects can be representative for two-phase flows involving liquid films of finite length. Besides, the flow near grooves and protrusions well indicates the role of the surface roughness, which is important for many applications.

References

Frank S. and Schwabe D. (1997): Temporal and spatial elements of thermocapillary convection in floating zone. *Experiments in Fluids*, vol. 23, pp. 234.

Irikira, M., Arakawa, Y., Ueno I., Kawamura H. (2005): Effect of ambient fluid flow upon onset of oscillatory thermocapillary convection in half-zone liquid bridge. *Microgravity Sci. Technol.*, vol. XVI-I, pp. 174.

Kamotani, Y., Wang, L., Hatta, S., Wang, A., Yoda S. (2003): Free surface heat loss effect on oscillatory thermocapillary flow in liquid bridges of high Prandtl number fluids, *Int. J. of Heat and Mass Transfer*, vol. 46, pp. 3211.

Kamotani Y., Matsumoto S. and Yoda S. (2007): Recent developments in oscillatory Marangoni convection. *FDMP: Fluid Dynamics & Materials Processing*, vol. 2, pp. 147.

Kuhlmann H.C. (1999): *Thermocapillary convection in models of crystal growth*, Berlin: Springer-Verlag.

Lombardi P.,De Angelis V., Banerjee S. (1996): Direct numerical simulations of near-interface turbulence in coupled gas-liquid flow. *Phys. Fluids*, vol. 8, pp. 1643.

Lappa M. (2004): *Fluids, Materials and Microgravity: Numerical Techniques and Insights into the Physics*, Elsevier Science Oxford, 538 pages.

Melnikov D., Shevtsova V., (2007): Axially running wave in liquid bridge, *FDMP: Fluid Dynamics & Materials Processing*, vol. 3, pp. 329.

Mialdun A., Shevtsova, V. M., (2006): Influence of interfacial heat exchange on the flow organization in liquid bridge. *Microgravity Sci. Technol.*, vol. XVIII-3/4, pp. 146.

Nishimura M., Ueno I., Nishino K., Kawamura H. (2005): 3D PTV measurement of oscillatory thermocapillary convection in half-zone liquid bridges. *Experiments in Fluids*, vol. 38, pp. 285.

Schetz A., Fuhs A.E. (1999): *Fundamentals of Fluid Mechanics*, Wiley-Interscience; 3rd edition.

Shevtsova, V., Mojahed M., Legros, J.C., (1999): The lost of stability in ground based experiments in liquid bridges, *Acta Astronautica*, vol. 44, pp. 625.

Shevtsova V., Mialdun A. and Mojahed M. (2005): A study of heat transfer in liquid bridges near onset of instability, *Int. J. of Non-equilibrium Thermodynamics*, vol. 30, pp. 261

Tiwari S. and Nishino K., (2007): Numerical study to investigate the effect of partition block and ambient air temperature on interfacial heat transfer in liquid bridges of high Prandtl number fluid. *J. Crystal Growth*, vol. 300, pp. 486.

Wang, A., Kamotani Y.,Yoda S. (2007a): Oscillatory thermocapillary flow in liquid bridges of high Prandtl number fluid with free surface heat gain, *Int. J. of Heat and Mass Transfer*, vol. 50, pp. 4195.

Yarin L.P., Mosyak A., Hestroni G. (2009): *Fluid flow, heat transfer and boiling in micro channels*, Berlin: Springer.